

Inelastic electroproduction of η_c at ep colliders

Li-Kun Hao and Feng Yuan

Department of Physics, Peking University, Beijing 100871, People's Republic of China

Kuang-Ta Chao

China Center of Advanced Science and Technology (World Laboratory), Beijing 100080, People's

Republic of China

and Department of Physics, Peking University, Beijing 100871, People's Republic of China

Abstract

Using the nonrelativistic QCD factorization formalism, we calculate the electroproduction cross sections of η_c in ep collisions, including the contribution from both the transverse photon and the longitudinal photon. For this process the color-singlet contribution vanishes up to the next to leading order perturbative QCD calculations. The dominant contribution comes from the color-octet $^1S_0^{(8)}$ subprocess. The nonperturbative color-octet matrix element of $^1S_0^{(8)}$ of η_c is related to that of $^3S_1^{(8)}$ of J/ψ by heavy quark spin symmetry, and the latter can be determined from the direct production of J/ψ at large transverse momentum at the Fermilab Tevatron. The measurement of this process at DESY HERA can be viewed as another independent test for the color-octet production mechanism.

PACS number(s): 12.40.Nn, 13.85.Ni, 14.40.Gx

Typeset using REVTeX

I. INTRODUCTION

Studies of heavy quarkonium production in high energy collisions may provide important information on both perturbative and nonperturbative QCD. Recent progress in this area was stimulated by the experimental results of the Collider Detector at Fermilab (**CDF**) at the Fermilab Tevatron. During the Tevatron run I, the **CDF** data [1] for the prompt production rates of J/ψ and ψ' at large transverse momentum were observed to be orders of magnitude larger than the lowest order perturbative calculation based on the color-singlet model [2]. At the same time, a new framework in treating quarkonium production and decays has been advocated by Bodwin, Braaten, and Lepage in the context of nonrelativistic quantum chromodynamics (NRQCD) [3]. In this approach, the production process is factorized into short and long distance parts, while the latter is associated with the nonperturbative matrix elements of four-fermion operators. So, for heavy quarkonium production, the quark-antiquark pair does not need to be in the color-singlet state in the short distance production stage, which occurs at the scale of $1/m_Q$ (m_Q being the heavy quark mass). At this stage, it allows a color configuration other than the singlet for the heavy quark pair, that is the color-octet. The later situation for heavy quarkonium production is called the color-octet mechanism. In this production mechanism, a heavy quark-antiquark pair is produced at short distances in a color-octet state, and then hadronizes into a final state quarkonium (the physical state) nonperturbatively. The color-octet terms in the gluon fragmentation to $J/\psi(\psi')$ have been considered to explain the $J/\psi(\psi')$ surplus problems discovered by CDF [4,5]. Taking the nonperturbative matrix elements $\langle \mathcal{O}_8^{J/\psi}({}^3S_1) \rangle$ and $\langle \mathcal{O}_8^{\psi'}({}^3S_1) \rangle$ as input parameters, the CDF surplus problem for J/ψ and ψ' can be explained as the contributions of color-octet terms due to gluon fragmentation. In the past few years, applications of the NRQCD factorization formalism to $J/\psi(\psi')$ production at various experimental facilities have been studied.

Even though the color-octet mechanism has achieved some successes in describing the production and decay of heavy quarkonia, more tests of this mechanism are still needed.

Recently, the photoproduction data from the DESY ep collider HERA [6] posed a question about the color-octet predictions for the inelastic photoproduction of J/ψ [7,8]. More recently, possible solutions for this problem have been suggested in [9–11]. In this situation it is certainly helpful to find other processes to test the color-octet mechanism in heavy quarkonium production. Under this context, we have studied η_c photoproduction in NRQCD [12]. We find that this process has several unique properties for the test of the color-octet production mechanism: (1) this process is purely a color-octet process up to the next to leading order in perturbative QCD; (2) this process is dominated by the $^1S_0^{(8)}$ channel, for which the color-octet matrix element can be related to the J/ψ hadroproduction at large p_T by the heavy quark spin symmetry; (3) unlike the inelastic J/ψ photoproduction which is affected by large diffraction background, the inelastic photoproduction of η_c has much lower diffraction background. So, the measurement of this process may clarify the existing conflict between the color-octet prediction and the experimental result on the J/ψ photoproduction. In this paper, we will extend our previous study of η_c production from the photoproduction region ($Q^2 \approx 0$) to the deep inelastic scattering (DIS) region ($Q^2 > 0$) at the energies relevant to the HERA collider. The electroproduction of η_c has the same features as the above mentioned for the test of the color-octet production mechanism.

Moreover, since Q^2 can be large, electroproduction is a better process from which to test the color-octet mechanism and to extract the NRQCD long distance matrix elements than photoproduction. The latter process lacks any large scale other than the charm quark mass, and consequently, perturbative corrections to leading order calculations are large. In addition, nonperturbative effects, such as higher twist corrections to the parton model, are less effectively suppressed in photoproduction than in electroproduction at large Q^2 .

The rest of the paper is organized as follows. In Sec. II, we give the cross section formula of η_c electroproduction in the color-octet model. In Sec. III, we give the numerical results about the production rates of η_c at the energy range relevant to HERA collider. The summary and discussions are given in Sec. IV.

II. η_c ELECTROPRODUCTION IN THE COLOR OCTET MODEL

The power of the NRQCD formalism stems from the fact that factorization formulas for observables are expansions in the small parameter v , where v is the average relative velocity of the heavy quark and antiquark in quarkonium bound state. For charmonium $v^2 \sim 0.3$, and for bottomonium $v^2 \sim 0.1$. NRQCD velocity-scaling rules [13] allow us to estimate the relative size of various NRQCD matrix elements. This information, along with the dependence of the short-distance coefficients on α_s and α , permits us to decide which terms must be retained in expressions for observables to reach a given level of accuracy. At low orders, factorization formulas involve only a few matrix elements, so several observables can be related by a small of parameters.

In NRQCD the Fock state expansion for η_c is

$$\begin{aligned}
 |\eta_c\rangle = & O(1)|c\bar{c}(^1S_0, \underline{1})\rangle + O(v)|c\bar{c}(^1P_1, \underline{8})g\rangle + O(v^2)|c\bar{c}(^3S_1, \underline{8} \text{ or } \underline{1})gg\rangle \\
 & + O(v^2)|c\bar{c}(^1S_0, \underline{8} \text{ or } \underline{1})gg\rangle + \dots.
 \end{aligned}
 \tag{1}$$

For the production of η_c , the contributions to the NRQCD matrix elements from the last three terms of the above expansion are the same order of v^2 according to the NRQCD velocity scaling rules. They are all suppressed by v^4 compared to the contribution from the first term (the color-singlet contribution). However, the color-singlet contributions to η_c production vanish in the leading order and the next to leading order γ^*g fusion processes (see the following). So, the production of η_c is purely a color-octet process, even to the next to leading order of QCD calculations. Therefore, the η_c production processes such as at the HERA, will provide an important test for the color-octet production mechanism. Furthermore, we will show by the following calculations, the dominant contribution to η_c production comes from the last term (color octet) of the Fock state expansion in Eq. (1). For this term, the associated color-octet production matrix element $\langle \mathcal{O}_8^{\eta_c}(^1S_0) \rangle$ can be related to the matrix element $\langle \mathcal{O}_8^\psi(^3S_1) \rangle$ by the heavy quark symmetry. And the latter color-octet matrix element is important for the color-octet explanation of the prompt J/ψ surplus

production at the Tevatron [4,5]. So, the measurement of η_c production processes is closely associated with the test of the color-octet gluon fragmentation mechanism proposed in [4].

The complete $ep \rightarrow \eta_c X$ cross section can be written as

$$\frac{d\sigma_{ep \rightarrow \eta_c X}(s)}{dydQ^2} = \Gamma(Q^2, y) d\sigma_{\gamma^* p \rightarrow \eta_c X}(W^2). \quad (2)$$

Here $\Gamma(Q^2, y)$ is the

$$\Gamma(Q^2, y) = \frac{\alpha}{2\pi Q^2 y} [1 + (1 - y)^2], \quad (3)$$

and

$$\sigma(\gamma^* p \rightarrow \eta_c X) = \sigma_T(\gamma^* p \rightarrow \eta_c X) + \sigma_L(\gamma^* p \rightarrow \eta_c X), \quad (4)$$

where σ_T and σ_L are the cross sections of virtual photon processes for the transverse polarized photon and longitudinal polarized photon respectively.

According to the NRQCD factorization formalism [3], the production process $\gamma^* + g \rightarrow \eta_c + X$ can be expressed as the following form,

$$d\sigma(\gamma^* + g \rightarrow \eta_c + X) = \sum_n F(\gamma^* + g \rightarrow n + X) \langle \mathcal{O}_n^{\eta_c} \rangle. \quad (5)$$

Here, n denotes the $c\bar{c}$ pair configuration in the expansion terms of Eq. (1) (including angular momentum $^{2S+1}L_J$ and color index 1 or 8). $F(\gamma^* + g \rightarrow n + X)$ is the short distance coefficient for the subprocess $\gamma^* + g \rightarrow n + X$. $\langle \mathcal{O}_n^{\eta_c} \rangle$ is the long distance non-perturbative matrix element which represents the probability of the $c\bar{c}$ pair in n configuration evolving into the physical state η_c . The short distance coefficient F can be calculated by using perturbative QCD in expansion of powers of α_s . The long distance matrix elements are still not available from the first principles at present. However, the relative importance of the contributions from different terms in Eq. (5) can be estimated by using the NRQCD velocity scaling rules.

From Eq. (1), we can see that the color-singlet contribution to the production of η_c is at the leading order in v^2 . The associated short distance coefficient is given by the subprocess

$$\gamma^* g \rightarrow c\bar{c}(^1S_0, \underline{1}) + g. \quad (6)$$

This process occurs at the next to leading order in α_s for the $\gamma^* g$ fusion processes. However, there is no contribution from this process, because it violates C (charge) parity conservation. (The C parities of the two gluon system (constrained in color-singlet) and the $c\bar{c}$ pair in ($^1S_0, \underline{1}$) state are both $+1$, while the C parity of the photon is -1).

The color-octet contributions to the η_c production come from the leading order and the next to leading order $\gamma^* g$ fusion processes as shown in Fig.1. At the leading order in α_s , the subprocess is $2 \rightarrow 1$ (Fig.1(a)),

$$\gamma^* g \rightarrow c\bar{c}(^1S_0, \underline{8}). \quad (7)$$

For this process, we readily have

$$\sigma(\gamma^* + g \rightarrow c\bar{c}(^1S_0, \underline{8}) \rightarrow \eta_c) = \frac{\pi^3 e_c^2 \alpha \alpha_s}{m_c^3} \delta(\hat{s} - 4m_c^2 - Q^2) \langle \mathcal{O}_8^{\eta_c}(^1S_0) \rangle, \quad (8)$$

where \hat{s} is the invariant mass squared of the partonic process. m_c is the charm quark mass, and we have approximated the charmonium bound state mass of η_c by $2m_c$.

At the next to leading order in α_s , the subprocesses are $2 \rightarrow 2$ (Fig.1(b) and Fig.1(c)). These processes contain the contributions from

$$\gamma^* + g \rightarrow c\bar{c}(^1S_0, \underline{8}) + g, \quad (9)$$

$$\gamma^* + g \rightarrow c\bar{c}(^3S_1, \underline{8}) + g, \quad (10)$$

$$\gamma^* + g \rightarrow c\bar{c}(^1P_1, \underline{8}) + g. \quad (11)$$

The cross sections for these $2 \rightarrow 2$ subprocesses can be expressed as the following form,

$$\frac{d\sigma}{d\hat{t}}(\gamma^* + g \rightarrow \eta_c + X) = \frac{1}{16\pi\hat{s}^2} F(^{2S+1}L_J^{(8)}) \langle \mathcal{O}_8^{\eta_c}(^{2S+1}L_J) \rangle, \quad (12)$$

where $\hat{t} = (z-1)\hat{s}$, and z is defined as $z = p \cdot k_{\eta_c} / p \cdot k_{\gamma^*}$ with p , k_{η_c} , k_{γ^*} being the momenta of the proton, the outgoing η_c and the incident photon respectively.

It is convenient to use the *helicity amplitude* method to calculate the cross section formulas for the virtual photon processes Eqs.(9-11). To the polarization vectors of the virtual photon, we choose

$$e_T = \frac{1}{\sqrt{2}}(0, 1, \pm i, 0), \quad e_L = \frac{1}{Q}p_1 + \frac{Q}{p_1 \cdot p_2}p_2, \quad (13)$$

for the transverse and longitudinal polarized photons respectively. For the incident and the outgoing gluons, following [14], we choose their polarization vectors as

$$\epsilon_2^{(\pm)} = N_e[\not{p}_2 \not{p}_3 \not{q}(1 \mp \gamma_5) + \not{q} \not{p}_3 \not{p}_2(1 \pm \gamma_5)], \quad (14)$$

$$\epsilon_3^{(\pm)} = N_e[\not{p}_3 \not{q} \not{p}_2(1 \mp \gamma_5) + \not{p}_2 \not{q} \not{p}_3(1 \pm \gamma_5)]. \quad (15)$$

Where $q = p_1 + \frac{Q^2}{2p_1 \cdot p_2}p_2$, $p_1^2 = -Q^2$ and p_1 is the momenta for the incident photon. p_2 , p_3 and e_2 , e_3 are the momenta and the polarization vectors for the incident gluon and outgoing gluon respectively. The normalization factor N_e is

$$N_e = \frac{1}{\sqrt{2(Q^2 M^2 + \hat{s}\hat{t})}}, \quad (16)$$

where M is the mass of η_c , the Mandelstam invariants \hat{s} , \hat{t} , \hat{u} are defined as

$$\hat{s} = (p_1 + p_2)^2, \quad \hat{t} = (p_2 - p_3)^2, \quad \hat{u} = (p_1 - p_3)^2, \quad (17)$$

and they satisfy the relation

$$\hat{s} + \hat{t} + \hat{u} = M^2 - Q^2 = 4m_c^2 - Q^2.$$

With these definitions for the polarization vectors of the photon and gluons Eqs. (13, 14, 15), the calculations of the helicity amplitudes are straightforward. The expressions for F 's in Eq.(12) are given in the Appendix.

III. NUMERICAL RESULTS

For the numerical evaluation, we choose $m_c = 1.5 \text{ GeV}$, and set the renormalization scale and the factorization scale both equal to $\mu^2 = (2m_c)^2 + Q^2$. For the parton distribution function of the proton, we use the Glück-Reya-Vogt (GRV) leading order (LO) parametrization [15].

Because there is no color-singlet contributions to η_c electroproduction up to the next to leading order perturbative calculations, we present in the following the numerical results only coming from the color-octet contributions. For the color-octet η_c production, by using the heavy quark spin symmetry, we estimate the associated color-octet matrix element $\langle \mathcal{O}_8^{\eta_c}(^1S_0) \rangle$ to be

$$\langle \mathcal{O}_8^{\eta_c}(^1S_0) \rangle \approx \langle \mathcal{O}_8^\psi(^3S_1) \rangle = 1.06 \times 10^{-2} GeV^3. \quad (18)$$

The value of the color-octet matrix element $\langle \mathcal{O}_8^{J/\psi}(^3S_1) \rangle$ follows the fitted value in [16] by comparing the theoretical prediction of direct J/ψ production to the experimental data at the Tevatron. For the other two color-octet matrix elements, we estimate their values by using the naive NRQCD velocity scaling rules,

$$\langle \mathcal{O}_8^{\eta_c}(^3S_1) \rangle \approx \langle \mathcal{O}_8^{\eta_c}(^1S_0) \rangle, \quad (19)$$

$$\langle \mathcal{O}_8^{\eta_c}(^1P_1) \rangle \approx \langle \mathcal{O}_8^{\eta_c}(^1S_0) \rangle. \quad (20)$$

In Fig.2, We first display the contribution from $2 \rightarrow 1$ partonic subprocess to the electroproduction of η_c , in which the intermediate color-octet state is $^1S_0^{(8)}$. The $2 \rightarrow 1$ process contributes to the η_c production in the forward direction ($z \sim 1$). In $e + p \rightarrow e + \eta_c + X$, we study the inelastic η_c production in the kinematic range of $4 < Q^2 < 80 GeV^2$ and $40 < W < 180 GeV^2$ for HERA experiments.

Next we study the $2 \rightarrow 2$ subprocesses contributions to the electroproduction of η_c . First, we consider the virtual photon-proton processes: $\gamma^*p \rightarrow \eta_c X$. In Fig.3, we plot the z distributions of the cross sections $\sigma_{tot}(\gamma^*p) = \sigma_T(\gamma^*p) + \sigma_L(\gamma^*p)$ of η_c production in the virtual photon-proton collisions at different values of Q^2 . Relevant to the HERA energy range, we choose the photon-proton c.m. energy $W = 100 GeV$ and select $Q^2 = 4, 10, 40 GeV^2$ to see the change of the cross sections with Q^2 . For comparison, we also show the photoproduction cross section in this figure ($Q^2 = 0$). From these plots, we can see that the shapes of the curves for the individual channel contributions do not change distinctly with Q^2 , and their relative importances also do not change. More important,

$^1S_0^{(8)}$ channel always dominates over the other two channels, which is the same as that in the photoproduction processes.

In Fig.4, we show the ratio $\sigma_L(\gamma^*p)/\sigma_T(\gamma^*p)$ as the function of z for $Q^2 = 10GeV^2$ and $40GeV^2$ respectively. We can see that this ratio increases in all channels as Q^2 increases. In particular, for the $^3S_1^{(8)}$ channel, as $z \rightarrow 1$, the ratio $\sigma_L(\gamma^*p)/\sigma_T(\gamma^*p)$ can reach a value over 4.4 for $Q^2 = 40GeV^2$. This is a distinct feature of the virtual photon with $Q^2 \gg m_c^2$. But the total cross section $\sigma_{tot}(\gamma^*p) = \sigma_L(\gamma^*p) + \sigma_T(\gamma^*p)$ coming from the $^3S_1^{(8)}$ channel decreases. The total cross section is always dominated by the $^1S_0^{(8)}$ channel for all value of Q^2 .

In Fig. 5, we show the cross sections of $e + p \rightarrow e + \eta_c + X$ at HERA. We plot the differential cross sections $d\sigma/dz$ as a function of z for two cases for the integration region of Q^2 : (a) $4GeV^2 < Q^2 < 80GeV^2$; (b) $20GeV^2 < Q^2 < 80GeV^2$.

From the above numerical results, we see that the contribution from the $^1S_0^{(8)}$ subprocess dominates the η_c electroproduction. The associated color-octet matrix element $\langle \mathcal{O}_8^{\eta_c}(^1S_0) \rangle$ can be related to the color-octet matrix element $\langle \mathcal{O}_8^{J/\psi}(^3S_1) \rangle$ by the heavy quark spin symmetry. The value of the later matrix element originates from the fitting to the large transverse momentum J/ψ production at the Fermilab Tevatron [16], which can be viewed as a reliable estimate. This is because the color-octet matrix element $\langle \mathcal{O}_8^{J/\psi}(^3S_1) \rangle$ dominantly contributes in the large p_T production [4,5,9], where the initial and final state gluon radiation effects are much smaller [9]. So, the η_c electroproduction together with its photoproduction can provide an important test for the color-octet production mechanism.

We note that the next to leading order QCD perturbative corrections are large for J/ψ photoproduction at HERA energy ranges [8,17,18]. These corrections change the normalization of the production rate by a factor of about 2. η_c photoproduction and electroproduction may also be affected by these corrections. However, the main features in testing the color-singlet and color-octet mechanisms mentioned above for η_c production will not be changed.

For the experimental observation of η_c , we suggest using all main decay channels of η_c

such as $\eta\pi\pi$, $\eta'\pi\pi$, $K\bar{K}\pi$, $\pi\pi\pi\pi$, $K\bar{K}\pi\pi$, $K\bar{K}K\bar{K}$, as well as $\gamma\gamma$ to detect η_c . The increase of luminosity at HERA offers the possibility of experimental investigation of electroproduction of η_c . In this connection, we note that photoproduction of the D_s meson has been observed through the $D_s \rightarrow \phi\pi$ channel at HERA [19]. According to our calculation, the photoproduction cross section of η_c is of the same order as the observed D_s . The branching ratio of $\eta_c \rightarrow K\bar{K}\pi$ or $\eta_c \rightarrow \phi\phi$ is comparable to that of $D_s \rightarrow \phi\pi$. Therefore, the experimental observation of photoproduction and leptonproduction of η_c might be possible through $\eta_c \rightarrow K\bar{K}\pi, \phi\phi$ decay modes in the near future.

IV. SUMMARY

We have calculated in this paper the inelastic η_c production in the electroproduction processes under the NRQCD factorization formalism. Same as the photoproduction of η_c [12], the color-singlet contributions to the electroproduction also vanish in the leading order and the next to leading order in perturbative QCD. The dominant contribution comes from the color-octet $^1S_0^{(8)}$ subprocess, for which the associated color-octet matrix element is related to the direct production of J/ψ at large transverse momentum at the Fermilab Tevatron. The measurement of this process at HERA can be viewed as another independent test for the color-octet production mechanism, and complement to the study of its photoproduction.

ACKNOWLEDGMENTS

This work was supported in part by the National Natural Science Foundation of China, the State Education Commission of China, and the State Commission of Science and Technology of China.

REFERENCES

- [1] CDF collaboration, F. Abe *et al.*, Phys. Rev. Lett. **69**, 3704 (1992); Phys. Rev. Lett. **71**, 2537 (1993); Phys. Rev. Lett. **79**, 572 (1997); Phys. Rev. Lett. **79**, 578 (1997)
- [2] R.Barbieri, R. Gatto, and E. Remiddi, Phys. Lett. 61B, 465 (1976); R.Barbieri, M. Caffo, and E. Remiddi, Nucl. Phys. B162, 220 (1980); R.Barbieri, M. Catto and E. Remiddi, Phys. Lett. 95B, 93 (1980); Phys. Lett. B 192,61 (1981).
- [3] G.T. Bodwin, L. Braaten, and G. P. Lepage, Phys. Rev. D51 1125 (1995).
- [4] E. Braaten and S. Fleming, Phys. Rev. Lett. **74**, 3327 (1995); M. Cacciari, M. Greco, M.L. Mangano and A. Petrelli, Phys. Lett. **B356** 553 (1995).
- [5] P. Cho and K. Leibovich, Phys. Rev. D**53**, 150 (1996); *ibid*, D**53**, 6203 (1996).
- [6] H1 Collaboration, S. Aid *et al*, Nucl. Phys. **B472**, 3 (1996); ZEUS Collaboration, M. Derrick *et al*, Z. Phys. C **599**, 612 (1997).
- [7] M. Cacciari and M. Krämer, Phys. Rev. Lett. **76**, 4128 (1996); P. Ko, J. Lee and H.S. Song, Phys. Rev. **D54**, 4312 (1996); J. Amundson, S. Fleming and I. Maksymyk, *ibid.* **56**, 5844 (1997).
- [8] M.Krämer, Nucl. Phys. **B459**, 3 (1996).
- [9] B. Cano-Coloma and M.A. Sanchis-Lozano, Nucl. Phys. **B508**, 753 (1997); B.A. Kniehl and G. Kramer, Eur. Phys. J. C 6, 493 (1999).
- [10] M. Beneke *et al.*, Phys. Lett. **B408**, 373 (1997).
- [11] K. Sridhar *et al.*, Phys. Lett. **B438**, 211 (1998).
- [12] L.K. Hao, F. Yuan, and K.T. Chao, Phys. Rev. Lett. **83**, 4490 (1999).
- [13] G.P.Lepage, L.Magnea, C.Nakhleh, U. Magnea, and K.Hornbostle, Phys. Rev. **D 46**, 4052(1992).

- [14] P.De Causmaecker, R.Gastmans, W.Troost, and T.T.Wu, Phys. Lett. **B105**, 215 (1981), Nucl. Phys. **B206**, 53 (1982); R.Gastmans, W.Troost, T.T.Wu, Nucl. Phys. **B291**, 731 (1987).
- [15] M. Glück et al. Z. Phys. **C67**, 433 (1995).
- [16] M. Beneke and M. Krämer, Phys. Rev.**D 55**, 5269 (1997).
- [17] M. Krämer, J. Zunft, J. Steegborg and P. M. Zerwas, Phys. Lett. **B 348**, 657 (1996).
- [18] F. Maltoni, M.L. Mangano and A. Petrelli, Nucl. Phys. **B519**, 361 (1998).
- [19] ZEUS Collaboration, J. Breirweg, Phys. Lett. B **481**, 213 (2000).

APPENDIX:

In this appendix, we list the cross sections for the different partonic processes.

For $^1S_0, ^3S_1$ and 1P_1 , the cross sections:

$$\begin{aligned}
 F(^3S_1^{(8)}) = & \frac{80(4\pi)^3 e_c^2 \alpha_s^2}{3(\hat{s} + \hat{t} + Q^2)^2 (\hat{s} + \hat{u} + 2Q^2)^2 (\hat{t} + \hat{u} + Q^2)^2 (Q^2 + s)^2} [3Q^{14} + 13Q^{12}\hat{s} + 11Q^{12}\hat{t} \\
 & + 7Q^{12}\hat{u} + 22Q^{10}\hat{s}^2 + 40Q^{10}\hat{s}\hat{t} + 30Q^{10}\hat{s}\hat{u} + 16Q^{10}\hat{t}^2 + 18Q^{10}\hat{t}\hat{u} + 5Q^{10}\hat{u}^2 \\
 & + 18Q^8\hat{s}^3 + 55Q^8\hat{s}^2\hat{t} + 50Q^8\hat{s}^2\hat{u} + 51Q^8\hat{s}\hat{t}^2 + 64Q^8\hat{s}\hat{t}\hat{u} + 21Q^8\hat{s}\hat{u}^2 + 12Q^8\hat{t}^3 \\
 & + 19Q^8\hat{t}^2\hat{u} + 8Q^8\hat{t}\hat{u}^2 + Q^8\hat{u}^3 + 7Q^6\hat{s}^4 + 35Q^6\hat{s}^3\hat{t} + 40Q^6\hat{s}^3\hat{u} + 61Q^6\hat{s}^2\hat{t}^2 \\
 & + 85Q^6\hat{s}^2\hat{t}\hat{u} + 34Q^6\hat{s}^2\hat{u}^2 + 31Q^6\hat{s}\hat{t}^3 + 56Q^6\hat{s}\hat{t}^2\hat{u} + 27Q^6\hat{s}\hat{t}\hat{u}^2 + 4Q^6\hat{s}\hat{u}^3 + 6Q^6\hat{t}^4 \\
 & + 11Q^6\hat{t}^3\hat{u} + 7Q^6\hat{t}^2\hat{u}^2 + Q^6\hat{t}\hat{u}^3 + Q^4\hat{s}^5 + 10Q^4\hat{s}^4\hat{t} + 15Q^4\hat{s}^4\hat{u} + 34Q^4\hat{s}^3\hat{t}^2 \\
 & + 51Q^4\hat{s}^3\hat{t}\hat{u} + 26Q^4\hat{s}^3\hat{u}^2 + 27Q^4\hat{s}^2\hat{t}^3 + 58Q^4\hat{s}^2\hat{t}^2\hat{u} + 33Q^4\hat{s}^2\hat{t}\hat{u}^2 + 6Q^4\hat{s}^2\hat{u}^3 \\
 & + 8Q^4\hat{s}\hat{t}^4 + 21Q^4\hat{s}\hat{t}^3\hat{u} + 17Q^4\hat{s}\hat{t}^2\hat{u}^2 + 3Q^4\hat{s}\hat{t}\hat{u}^3 + 2Q^4\hat{t}^5 + 4Q^4\hat{t}^4\hat{u} + 3Q^4\hat{t}^3\hat{u}^2 \\
 & + Q^4\hat{t}^2\hat{u}^3 + Q^2\hat{s}^5\hat{t} + 2Q^2\hat{s}^5\hat{u} + 9Q^2\hat{s}^4\hat{t}^2 + 13Q^2\hat{s}^4\hat{t}\hat{u} + 9Q^2\hat{s}^4\hat{u}^2 + 9Q^2\hat{s}^3\hat{t}^3 \\
 & + 24Q^2\hat{s}^3\hat{t}^2\hat{u} + 17Q^2\hat{s}^3\hat{t}\hat{u}^2 + 4Q^2\hat{s}^3\hat{u}^3 + 2Q^2\hat{s}^2\hat{t}^4 + 11Q^2\hat{s}^2\hat{t}^3\hat{u} + 13Q^2\hat{s}^2\hat{t}^2\hat{u}^2 \\
 & + 3Q^2\hat{s}^2\hat{t}\hat{u}^3 + 2Q^2\hat{s}\hat{t}^4\hat{u} + 4Q^2\hat{s}\hat{t}^3\hat{u}^2 + 2Q^2\hat{s}\hat{t}^2\hat{u}^3 + \hat{s}^5\hat{t}^2 + \hat{s}^5\hat{t}\hat{u} + \hat{s}^5\hat{u}^2 + \hat{s}^4\hat{t}^3 \\
 & + 3\hat{s}^4\hat{t}^2\hat{u} + 3\hat{s}^4\hat{t}\hat{u}^2 + \hat{s}^4\hat{u}^3 + \hat{s}^3\hat{t}^3\hat{u} + 3\hat{s}^3\hat{t}^2\hat{u}^2 + \hat{s}^3\hat{t}\hat{u}^3 + \hat{s}^2\hat{t}^3\hat{u}^2 + \hat{s}^2\hat{t}^2\hat{u}^3]. \quad (A1)
 \end{aligned}$$

$$\begin{aligned}
 F(^1S_0^{(8)}) = & \frac{24(4\pi)^3 e_c^2 \alpha_s^2}{(Q^2 + \hat{s} + \hat{t})^2 (2Q^2 + \hat{s} + \hat{u})^2 (Q^2 + \hat{s})^2 (Q^2 + \hat{t} + \hat{u})^2} [9Q^{16} + 45Q^{14}\hat{s} + 49Q^{14}\hat{t} \\
 & + 27Q^{14}\hat{u} + 96Q^{12}\hat{s}^2 + 174Q^{12}\hat{s}\hat{t} + 123Q^{12}\hat{s}\hat{u} + 94Q^{12}\hat{t}^2 + 136Q^{12}\hat{t}\hat{u} + 33Q^{12}\hat{u}^2 \\
 & + 114Q^{10}\hat{s}^3 + 256Q^{10}\hat{s}^2\hat{t} + 234Q^{10}\hat{s}^2\hat{u} + 250Q^{10}\hat{s}\hat{t}^2 + 430Q^{10}\hat{s}\hat{t}\hat{u} + 135Q^{10}\hat{s}\hat{u}^2 \\
 & + 80Q^{10}\hat{t}^3 + 202Q^{10}\hat{t}^2\hat{u} + 145Q^{10}\hat{t}\hat{u}^2 + 21Q^{10}\hat{u}^3 + 82Q^8\hat{s}^4 + 206Q^8\hat{s}^3\hat{t} \\
 & + 242Q^8\hat{s}^3\hat{u} + 273Q^8\hat{s}^2\hat{t}^2 + 538Q^8\hat{s}^2\hat{t}\hat{u} + 222Q^8\hat{s}^2\hat{u}^2 + 172Q^8\hat{s}\hat{t}^3 + 462Q^8\hat{s}\hat{t}^2\hat{u} \\
 & + 406Q^8\hat{s}\hat{t}\hat{u}^2 + 77Q^8\hat{s}\hat{u}^3 + 31Q^8\hat{t}^4 + 112Q^8\hat{t}^3\hat{u} + 145Q^8\hat{t}^2\hat{u}^2 + 70Q^8\hat{t}\hat{u}^3 + 7Q^8\hat{u}^4 \\
 & + 36Q^6\hat{s}^5 + 98Q^6\hat{s}^4\hat{t} + 148Q^6\hat{s}^4\hat{u} + 157Q^6\hat{s}^3\hat{t}^2 + 352Q^6\hat{s}^3\hat{t}\hat{u} + 188Q^6\hat{s}^3\hat{u}^2 \\
 & + 153Q^6\hat{s}^2\hat{t}^3 + 413Q^6\hat{s}^2\hat{t}^2\hat{u} + 420Q^6\hat{s}^2\hat{t}\hat{u}^2 + 108Q^6\hat{s}^2\hat{u}^3 + 63Q^6\hat{s}\hat{t}^4 + 194Q^6\hat{s}\hat{t}^3\hat{u} \\
 & + 275Q^6\hat{s}\hat{t}^2\hat{u}^2 + 172Q^6\hat{s}\hat{t}\hat{u}^3 + 23Q^6\hat{s}\hat{u}^4 + 5Q^6\hat{t}^5 + 21Q^6\hat{t}^4\hat{u} + 39Q^6\hat{t}^3\hat{u}^2
 \end{aligned}$$

$$\begin{aligned}
& +35Q^6\hat{t}^2\hat{u}^3 + 13Q^6\hat{t}\hat{u}^4 + Q^6\hat{u}^5 + 9Q^4\hat{s}^6 + 26Q^4\hat{s}^5\hat{t} + 54Q^4\hat{s}^5\hat{u} + 45Q^4\hat{s}^4\hat{t}^2 \\
& +132Q^4\hat{s}^4\hat{t}\hat{u} + 87Q^4\hat{s}^4\hat{u}^2 + 60Q^4\hat{s}^3\hat{t}^3 + 191Q^4\hat{s}^3\hat{t}^2\hat{u} + 208Q^4\hat{s}^3\hat{t}\hat{u}^2 + 72Q^4\hat{s}^3\hat{u}^3 \\
& +43Q^4\hat{s}^2\hat{t}^4 + 134Q^4\hat{s}^2\hat{t}^3\hat{u} + 181Q^4\hat{s}^2\hat{t}^2\hat{u}^2 + 140Q^4\hat{s}^2\hat{t}\hat{u}^3 + 27Q^4\hat{s}^2\hat{u}^4 + 10Q^4\hat{s}\hat{t}^5 \\
& +33Q^4\hat{s}\hat{t}^4\hat{u} + 50Q^4\hat{s}\hat{t}^3\hat{u}^2 + 53Q^4\hat{s}\hat{t}^2\hat{u}^3 + 28Q^4\hat{s}\hat{t}\hat{u}^4 + 3Q^4\hat{s}\hat{u}^5 + Q^2\hat{s}^7 + 3Q^2\hat{s}^6\hat{t} \\
& +11Q^2\hat{s}^6\hat{u} + 5Q^2\hat{s}^5\hat{t}^2 + 26Q^2\hat{s}^5\hat{t}\hat{u} + 21Q^2\hat{s}^5\hat{u}^2 + 9Q^2\hat{s}^4\hat{t}^3 + 41Q^2\hat{s}^4\hat{t}^2\hat{u} \\
& +55Q^2\hat{s}^4\hat{t}\hat{u}^2 + 23Q^2\hat{s}^4\hat{u}^3 + 11Q^2\hat{s}^3\hat{t}^4 + 34Q^2\hat{s}^3\hat{t}^3\hat{u} + 57Q^2\hat{s}^3\hat{t}^2\hat{u}^2 + 44Q^2\hat{s}^3\hat{t}\hat{u}^3 \\
& +13Q^2\hat{s}^3\hat{u}^4 + 5Q^2\hat{s}^2\hat{t}^5 + 13Q^2\hat{s}^2\hat{t}^4\hat{u} + 23Q^2\hat{s}^2\hat{t}^3\hat{u}^2 + 21Q^2\hat{s}^2\hat{t}^2\hat{u}^3 + 17Q^2\hat{s}^2\hat{t}\hat{u}^4 \\
& +3Q^2\hat{s}^2\hat{u}^5 + \hat{s}^7\hat{u} + 2\hat{s}^6\hat{t}\hat{u} + 2\hat{s}^6\hat{u}^2 + 3\hat{s}^5\hat{t}^2\hat{u} + 6\hat{s}^5\hat{t}\hat{u}^2 + 3\hat{s}^5\hat{u}^3 + 2\hat{s}^4\hat{t}^3\hat{u} + 6\hat{s}^4\hat{t}^2\hat{u}^2 \\
& +6\hat{s}^4\hat{t}\hat{u}^3 + 2\hat{s}^4\hat{u}^4 + \hat{s}^3\hat{t}^4\hat{u} + 2\hat{s}^3\hat{t}^3\hat{u}^2 + 3\hat{s}^3\hat{t}^2\hat{u}^3 + 2\hat{s}^3\hat{t}\hat{u}^4 + \hat{s}^3\hat{u}^5]. \tag{A2}
\end{aligned}$$

$$\begin{aligned}
F(^1P_1^{(8)}) = & \frac{320(4\pi)^3 e_c^2 \alpha_s^2}{3(2m_c)^2(Q^2 + \hat{s} + \hat{t})^3(2Q^2 + \hat{s} + \hat{u})^4(Q^2 + \hat{t} + \hat{u})^3(Q^2 + \hat{s})^2} \\
& [48Q^{22} + 336Q^{20}\hat{s} + 336Q^{20}\hat{t} + 240Q^{20}\hat{u} + 1048Q^{18}\hat{s}^2 + 1900Q^{18}\hat{s}\hat{t} + 1552Q^{18}\hat{s}\hat{u} \\
& +922Q^{18}\hat{t}^2 + 1548Q^{18}\hat{t}\hat{u} + 520Q^{18}\hat{u}^2 + 1920Q^{16}\hat{s}^3 + 4716Q^{16}\hat{s}^2\hat{t} + 4432Q^{16}\hat{s}^2\hat{u} \\
& +4304Q^{16}\hat{s}\hat{t}^2 + 7960Q^{16}\hat{s}\hat{t}\hat{u} + 3088Q^{16}\hat{s}\hat{u}^2 + 1410Q^{16}\hat{t}^3 + 3700Q^{16}\hat{t}^2\hat{u} \\
& +3044Q^{16}\hat{t}\hat{u}^2 + 640Q^{16}\hat{u}^3 + 2291Q^{14}\hat{s}^4 + 6795Q^{14}\hat{s}^3\hat{t} + 7356Q^{14}\hat{s}^3\hat{u} \\
& +8702Q^{14}\hat{s}^2\hat{t}^2 + 17713Q^{14}\hat{s}^2\hat{t}\hat{u} + 7994Q^{14}\hat{s}^2\hat{u}^2 + 5498Q^{14}\hat{s}\hat{t}^3 + 15470Q^{14}\hat{s}\hat{t}^2\hat{u} \\
& +14125Q^{14}\hat{s}\hat{t}\hat{u}^2 + 3468Q^{14}\hat{s}\hat{u}^3 + 1518Q^{14}\hat{t}^4 + 4898Q^{14}\hat{t}^3\hat{u} + 6220Q^{14}\hat{t}^2\hat{u}^2 \\
& +3319Q^{14}\hat{t}\hat{u}^3 + 491Q^{14}\hat{u}^4 + 1863Q^{12}\hat{s}^5 + 6339Q^{12}\hat{s}^4\hat{t} + 7853Q^{12}\hat{s}^4\hat{u} \\
& +10120Q^{12}\hat{s}^3\hat{t}^2 + 22468Q^{12}\hat{s}^3\hat{t}\hat{u} + 11838Q^{12}\hat{s}^3\hat{u}^2 + 9156Q^{12}\hat{s}^2\hat{t}^3 + 27460Q^{12}\hat{s}^2\hat{t}^2\hat{u} \\
& +27824Q^{12}\hat{s}^2\hat{t}\hat{u}^2 + 8050Q^{12}\hat{s}^2\hat{u}^3 + 4972Q^{12}\hat{s}\hat{t}^4 + 16826Q^{12}\hat{s}\hat{t}^3\hat{u} + 22970Q^{12}\hat{s}\hat{t}^2\hat{u}^2 \\
& +13768Q^{12}\hat{s}\hat{t}\hat{u}^3 + 2411Q^{12}\hat{s}\hat{u}^4 + 1334Q^{12}\hat{t}^5 + 4676Q^{12}\hat{t}^4\hat{u} + 7100Q^{12}\hat{t}^3\hat{u}^2 \\
& +5690Q^{12}\hat{t}^2\hat{u}^3 + 2177Q^{12}\hat{t}\hat{u}^4 + 241Q^{12}\hat{u}^5 + 1047Q^{10}\hat{s}^6 + 4042Q^{10}\hat{s}^5\hat{t} \\
& +5628Q^{10}\hat{s}^5\hat{u} + 7609Q^{10}\hat{s}^4\hat{t}^2 + 18020Q^{10}\hat{s}^4\hat{t}\hat{u} + 11052Q^{10}\hat{s}^4\hat{u}^2 \\
& +8639Q^{10}\hat{s}^3\hat{t}^3 + 27282Q^{10}\hat{s}^3\hat{t}^2\hat{u} + 30485Q^{10}\hat{s}^3\hat{t}\hat{u}^2 + 10452Q^{10}\hat{s}^3\hat{u}^3 + 6717Q^{10}\hat{s}^2\hat{t}^4 \\
& +23967Q^{10}\hat{s}^2\hat{t}^3\hat{u} + 35078Q^{10}\hat{s}^2\hat{t}^2\hat{u}^2 + 23615Q^{10}\hat{s}^2\hat{t}\hat{u}^3 + 4955Q^{10}\hat{s}^2\hat{u}^4]
\end{aligned}$$

$$\begin{aligned}
&+3568Q^{10}\hat{s}\hat{t}^5 + 13176Q^{10}\hat{s}\hat{t}^4\hat{u} + 20989Q^{10}\hat{s}\hat{t}^3\hat{u}^2 + 18212Q^{10}\hat{s}\hat{t}^2\hat{u}^3 + 7977Q^{10}\hat{s}\hat{t}\hat{u}^4 \\
&+1064Q^{10}\hat{s}\hat{u}^5 + 902Q^{10}\hat{t}^6 + 3520Q^{10}\hat{t}^5\hat{u} + 5917Q^{10}\hat{t}^4\hat{u}^2 + 5581Q^{10}\hat{t}^3\hat{u}^3 \\
&+3079Q^{10}\hat{t}^2\hat{u}^4 + 869Q^{10}\hat{t}\hat{u}^5 + 74Q^{10}\hat{u}^6 + 402Q^8\hat{s}^7 + 1807Q^8\hat{s}^6\hat{t} \\
&+2736Q^8\hat{s}^6\hat{u} + 3946Q^8\hat{s}^5\hat{t}^2 + 9568Q^8\hat{s}^5\hat{t}\hat{u} + 6747Q^8\hat{s}^5\hat{u}^2 + 5199Q^8\hat{s}^4\hat{t}^3 \\
&+16875Q^8\hat{s}^4\hat{t}^2\hat{u} + 20452Q^8\hat{s}^4\hat{t}\hat{u}^2 + 8305Q^8\hat{s}^4\hat{u}^3 + 4895Q^8\hat{s}^3\hat{t}^4 + 18541Q^8\hat{s}^3\hat{t}^3\hat{u} \\
&+28923Q^8\hat{s}^3\hat{t}^2\hat{u}^2 + 21762Q^8\hat{s}^3\hat{t}\hat{u}^3 + 5520Q^8\hat{s}^3\hat{u}^4 + 3687Q^8\hat{s}^2\hat{t}^5 + 14625Q^8\hat{s}^2\hat{t}^4\hat{u} \\
&+24778Q^8\hat{s}^2\hat{t}^3\hat{u}^2 + 23241Q^8\hat{s}^2\hat{t}^2\hat{u}^3 + 11647Q^8\hat{s}^2\hat{t}\hat{u}^4 + 1906Q^8\hat{s}^2\hat{u}^5 + 1848Q^8\hat{s}\hat{t}^6 \\
&+7722Q^8\hat{s}\hat{t}^5\hat{u} + 13765Q^8\hat{s}\hat{t}^4\hat{u}^2 + 13745Q^8\hat{s}\hat{t}^3\hat{u}^3 + 8329Q^8\hat{s}\hat{t}^2\hat{u}^4 + 2770Q^8\hat{s}\hat{t}\hat{u}^5 \\
&+291Q^8\hat{s}\hat{u}^6 + 398Q^8\hat{t}^7 + 1804Q^8\hat{t}^6\hat{u} + 3523Q^8\hat{t}^5\hat{u}^2 + 3855Q^8\hat{t}^4\hat{u}^3 + 2547Q^8\hat{t}^3\hat{u}^4 \\
&+998Q^8\hat{t}^2\hat{u}^5 + 202Q^8\hat{t}\hat{u}^6 + 13Q^8\hat{u}^7 + 101Q^6\hat{s}^8 + 567Q^6\hat{s}^7\hat{t} + 887Q^6\hat{s}^7\hat{u} \\
&+1458Q^6\hat{s}^6\hat{t}^2 + 3403Q^6\hat{s}^6\hat{t}\hat{u} + 2693Q^6\hat{s}^6\hat{u}^2 + 2141Q^6\hat{s}^5\hat{t}^3 + 6828Q^6\hat{s}^5\hat{t}^2\hat{u} \\
&+8693Q^6\hat{s}^5\hat{t}\hat{u}^2 + 4139Q^6\hat{s}^5\hat{u}^3 + 2154Q^6\hat{s}^4\hat{t}^4 + 8625Q^6\hat{s}^4\hat{t}^3\hat{u} + 14103Q^6\hat{s}^4\hat{t}^2\hat{u}^2 \\
&+11713Q^6\hat{s}^4\hat{t}\hat{u}^3 + 3600Q^6\hat{s}^4\hat{u}^4 + 1868Q^6\hat{s}^3\hat{t}^5 + 8205Q^6\hat{s}^3\hat{t}^4\hat{u} + 14993Q^6\hat{s}^3\hat{t}^3\hat{u}^2 \\
&+15220Q^6\hat{s}^3\hat{t}^2\hat{u}^3 + 8678Q^6\hat{s}^3\hat{t}\hat{u}^4 + 1769Q^6\hat{s}^3\hat{u}^5 + 1337Q^6\hat{s}^2\hat{t}^6 + 6118Q^6\hat{s}^2\hat{t}^5\hat{u} \\
&+11895Q^6\hat{s}^2\hat{t}^4\hat{u}^2 + 12811Q^6\hat{s}^2\hat{t}^3\hat{u}^3 + 8502Q^6\hat{s}^2\hat{t}^2\hat{u}^4 + 3332Q^6\hat{s}^2\hat{t}\hat{u}^5 + 445Q^6\hat{s}^2\hat{u}^6 \\
&+570Q^6\hat{s}\hat{t}^7 + 2792Q^6\hat{s}\hat{t}^6\hat{u} + 5910Q^6\hat{s}\hat{t}^5\hat{u}^2 + 6989Q^6\hat{s}\hat{t}^4\hat{u}^3 + 5004Q^6\hat{s}\hat{t}^3\hat{u}^4 \\
&+2210Q^6\hat{s}\hat{t}^2\hat{u}^5 + 550Q^6\hat{s}\hat{t}\hat{u}^6 + 45Q^6\hat{s}\hat{u}^7 + 98Q^6\hat{t}^8 + 514Q^6\hat{t}^7\hat{u} + 1187Q^6\hat{t}^6\hat{u}^2 \\
&+1572Q^6\hat{t}^5\hat{u}^3 + 1287Q^6\hat{t}^4\hat{u}^4 + 646Q^6\hat{t}^3\hat{u}^5 + 183Q^6\hat{t}^2\hat{u}^6 + 24Q^6\hat{t}\hat{u}^7 + Q^6\hat{u}^8 \\
&+15Q^4\hat{s}^9 + 121Q^4\hat{s}^8\hat{t} + 182Q^4\hat{s}^8\hat{u} + 379Q^4\hat{s}^7\hat{t}^2 + 791Q^4\hat{s}^7\hat{t}\hat{u} + 677Q^4\hat{s}^7\hat{u}^2 \\
&+620Q^4\hat{s}^6\hat{t}^3 + 1823Q^4\hat{s}^6\hat{t}^2\hat{u} + 2317Q^4\hat{s}^6\hat{t}\hat{u}^2 + 1265Q^4\hat{s}^6\hat{u}^3 + 623Q^4\hat{s}^5\hat{t}^4 \\
&+2536Q^4\hat{s}^5\hat{t}^3\hat{u} + 4166Q^4\hat{s}^5\hat{t}^2\hat{u}^2 + 3725Q^4\hat{s}^5\hat{t}\hat{u}^3 + 1376Q^4\hat{s}^5\hat{u}^4 \\
&+498Q^4\hat{s}^4\hat{t}^5 + 2545Q^4\hat{s}^4\hat{t}^4\hat{u} + 4986Q^4\hat{s}^4\hat{t}^3\hat{u}^2 + 5449Q^4\hat{s}^4\hat{t}^2\hat{u}^3 \\
&+3502Q^4\hat{s}^4\hat{t}\hat{u}^4 + 896Q^4\hat{s}^4\hat{u}^5 + 393Q^4\hat{s}^3\hat{t}^6 + 2150Q^4\hat{s}^3\hat{t}^5\hat{u} + 4713Q^4\hat{s}^3\hat{t}^4\hat{u}^2 \\
&+5603Q^4\hat{s}^3\hat{t}^3\hat{u}^3 + 4117Q^4\hat{s}^3\hat{t}^2\hat{u}^4 + 1881Q^4\hat{s}^3\hat{t}\hat{u}^5 + 329Q^4\hat{s}^3\hat{u}^6 + 237Q^4\hat{s}^2\hat{t}^7
\end{aligned}$$

$$\begin{aligned}
&+1343Q^4s^2t^6\hat{u} + 3229Q^4s^2t^5\hat{u}^2 + 4283Q^4s^2t^4\hat{u}^3 + 3395Q^4s^2t^3\hat{u}^4 \\
&+1683Q^4s^2t^2\hat{u}^5 + 519Q^4s^2t\hat{u}^6 + 57Q^4s^2\hat{u}^7 + 76Q^4s\hat{t}^8 + 460Q^4s\hat{t}^7\hat{u} \\
&+1205Q^4s\hat{t}^6\hat{u}^2 + 1804Q^4s\hat{t}^5\hat{u}^3 + 1670Q^4s\hat{t}^4\hat{u}^4 + 955Q^4s\hat{t}^3\hat{u}^5 \\
&+320Q^4s\hat{t}^2\hat{u}^6 + 55Q^4s\hat{t}\hat{u}^7 + 3Q^4s\hat{u}^8 + 10Q^4t^9 + 60Q^4t^8\hat{u} + 161Q^4t^7\hat{u}^2 \\
&+255Q^4t^6\hat{u}^3 + 261Q^4t^5\hat{u}^4 + 174Q^4t^4\hat{u}^5 + 71Q^4t^3\hat{u}^6 + 15Q^4t^2\hat{u}^7 + Q^4t\hat{u}^8 \\
&+Q^2s^{10} + 16Q^2s^9t + 21Q^2s^9\hat{u} + 63Q^2s^8t^2 + 110Q^2s^8t\hat{u} + 97Q^2s^8\hat{u}^2 \\
&+118Q^2s^7t^3 + 302Q^2s^7t^2\hat{u} + 359Q^2s^7t\hat{u}^2 + 217Q^2s^7\hat{u}^3 + 125Q^2s^6t^4 \\
&+466Q^2s^6t^3\hat{u} + 715Q^2s^6t^2\hat{u}^2 + 659Q^2s^6t\hat{u}^3 + 286Q^2s^6\hat{u}^4 + 84Q^2s^5t^5 \\
&+461Q^2s^5t^4\hat{u} + 910Q^2s^5t^3\hat{u}^2 + 1032Q^2s^5t^2\hat{u}^3 + 735Q^2s^5t\hat{u}^4 + 235Q^2s^5\hat{u}^5 \\
&+47Q^2s^4t^6 + 344Q^2s^4t^5\hat{u} + 876Q^2s^4t^4\hat{u}^2 + 1148Q^2s^4t^3\hat{u}^3 + 949Q^2s^4t^2\hat{u}^4 \\
&+501Q^2s^4t\hat{u}^5 + 117Q^2s^4\hat{u}^6 + 26Q^2s^3t^7 + 206Q^2s^3t^6\hat{u} + 640Q^2s^3t^5\hat{u}^2 \\
&+999Q^2s^3t^4\hat{u}^3 + 916Q^2s^3t^3\hat{u}^4 + 528Q^2s^3t^2\hat{u}^5 + 196Q^2s^3t\hat{u}^6 + 31Q^2s^3\hat{u}^7 \\
&+8Q^2s^2t^8 + 78Q^2s^2t^7\hat{u} + 289Q^2s^2t^6\hat{u}^2 + 542Q^2s^2t^5\hat{u}^3 + 599Q^2s^2t^4\hat{u}^4 \\
&+402Q^2s^2t^3\hat{u}^5 + 161Q^2s^2t^2\hat{u}^6 + 38Q^2s^2t\hat{u}^7 + 3Q^2s^2\hat{u}^8 + 10Q^2s\hat{t}^8\hat{u} + 52Q^2s\hat{t}^7\hat{u}^2 \\
&+120Q^2s\hat{t}^6\hat{u}^3 + 162Q^2s\hat{t}^5\hat{u}^4 + 138Q^2s\hat{t}^4\hat{u}^5 + 72Q^2s\hat{t}^3\hat{u}^6 + 20Q^2s\hat{t}^2\hat{u}^7 + 2Q^2s\hat{t}\hat{u}^8 \\
&+\hat{s}^{10}\hat{t} + \hat{s}^{10}\hat{u} + 5\hat{s}^9\hat{t}^2 + 7\hat{s}^9\hat{t}\hat{u} + 6\hat{s}^9\hat{u}^2 + 11\hat{s}^8\hat{t}^3 + 24\hat{s}^8\hat{t}^2\hat{u} + 25\hat{s}^8\hat{t}\hat{u}^2 \\
&+16\hat{s}^8\hat{u}^3 + 14\hat{s}^7\hat{t}^4 + 43\hat{s}^7\hat{t}^3\hat{u} + 57\hat{s}^7\hat{t}^2\hat{u}^2 + 51\hat{s}^7\hat{t}\hat{u}^3 + 25\hat{s}^7\hat{u}^4 + 11\hat{s}^6\hat{t}^5 + 46\hat{s}^6\hat{t}^4\hat{u} \\
&+78\hat{s}^6\hat{t}^3\hat{u}^2 + 84\hat{s}^6\hat{t}^2\hat{u}^3 + 64\hat{s}^6\hat{t}\hat{u}^4 + 25\hat{s}^6\hat{u}^5 + 5\hat{s}^5\hat{t}^6 + 30\hat{s}^5\hat{t}^5\hat{u} + 70\hat{s}^5\hat{t}^4\hat{u}^2 \\
&+92\hat{s}^5\hat{t}^3\hat{u}^3 + 84\hat{s}^5\hat{t}^2\hat{u}^4 + 51\hat{s}^5\hat{t}\hat{u}^5 + 16\hat{s}^5\hat{u}^6 + \hat{s}^4\hat{t}^7 + 11\hat{s}^4\hat{t}^6\hat{u} + 38\hat{s}^4\hat{t}^5\hat{u}^2 + 70\hat{s}^4\hat{t}^4\hat{u}^3 \\
&+78\hat{s}^4\hat{t}^3\hat{u}^4 + 57\hat{s}^4\hat{t}^2\hat{u}^5 + 25\hat{s}^4\hat{t}\hat{u}^6 + 6\hat{s}^4\hat{u}^7 + 2\hat{s}^3\hat{t}^7\hat{u} + 11\hat{s}^3\hat{t}^6\hat{u}^2 + 30\hat{s}^3\hat{t}^5\hat{u}^3 \\
&+46\hat{s}^3\hat{t}^4\hat{u}^4 + 43\hat{s}^3\hat{t}^3\hat{u}^5 + 24\hat{s}^3\hat{t}^2\hat{u}^6 + 7\hat{s}^3\hat{t}\hat{u}^7 + \hat{s}^3\hat{u}^8 + \hat{s}^2\hat{t}^7\hat{u}^2 + 5\hat{s}^2\hat{t}^6\hat{u}^3 + 11\hat{s}^2\hat{t}^5\hat{u}^4 \\
&+14\hat{s}^2\hat{t}^4\hat{u}^5 + 11\hat{s}^2\hat{t}^3\hat{u}^6 + 5\hat{s}^2\hat{t}^2\hat{u}^7 + \hat{s}^2\hat{t}\hat{u}^8].
\end{aligned} \tag{A3}$$

Figure Captions

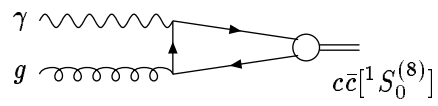
FIG. 1. The Feynman diagrams for the production of η_c at the leading order (a) and the next to leading order (b) and (c) γ^*g fusion processes. All of these diagrams are for the color-octet processes.

FIG. 2. The cross section $d\sigma/dQ^2$ for the process $e + p \rightarrow e + \eta_c + X$ in the forward direction ($z \sim 1$) as a function of Q^2 . where $\sqrt{s_{ep}} = 300\text{GeV}$.

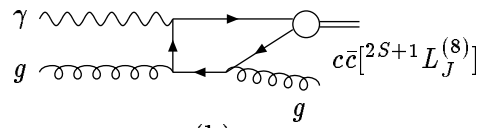
FIG. 3. The differential cross sections $d\sigma/dz$ for the process $\gamma^* + p \rightarrow \eta_c + X$ at the HERA as a function of $z \equiv E_{\eta_c}/E_{\gamma^*}$, where $W_{\gamma^*p} = 100\text{GeV}$; (a) $Q^2 = 0\text{GeV}^2$; (b) $Q^2 = 4\text{GeV}^2$; (c) $Q^2 = 10\text{GeV}^2$; (d) $Q^2 = 40\text{GeV}^2$. The curves denote contributions from the color-octet 1S_0 , 1P_1 , and 3S_1 respectively.

FIG. 4. The ratio $\sigma_L(\gamma^*p)/\sigma_T(\gamma^*p)$ as the function of z . (a) $Q^2 = 10\text{GeV}^2$. (b) $Q^2 = 40\text{GeV}^2$.

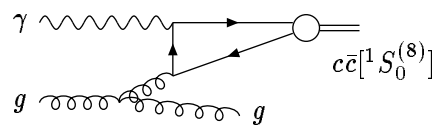
FIG. 5. The cross section $d\sigma/dz$ for $e + p \rightarrow e + \eta_c + X$ at HERA as a function of z , where $\sqrt{s_{ep}} = 300\text{GeV}$. (a) $4\text{GeV}^2 < Q^2 < 80\text{GeV}^2$, (b) $20\text{GeV}^2 < Q^2 < 80\text{GeV}^2$.



(a)



(b)



(c)

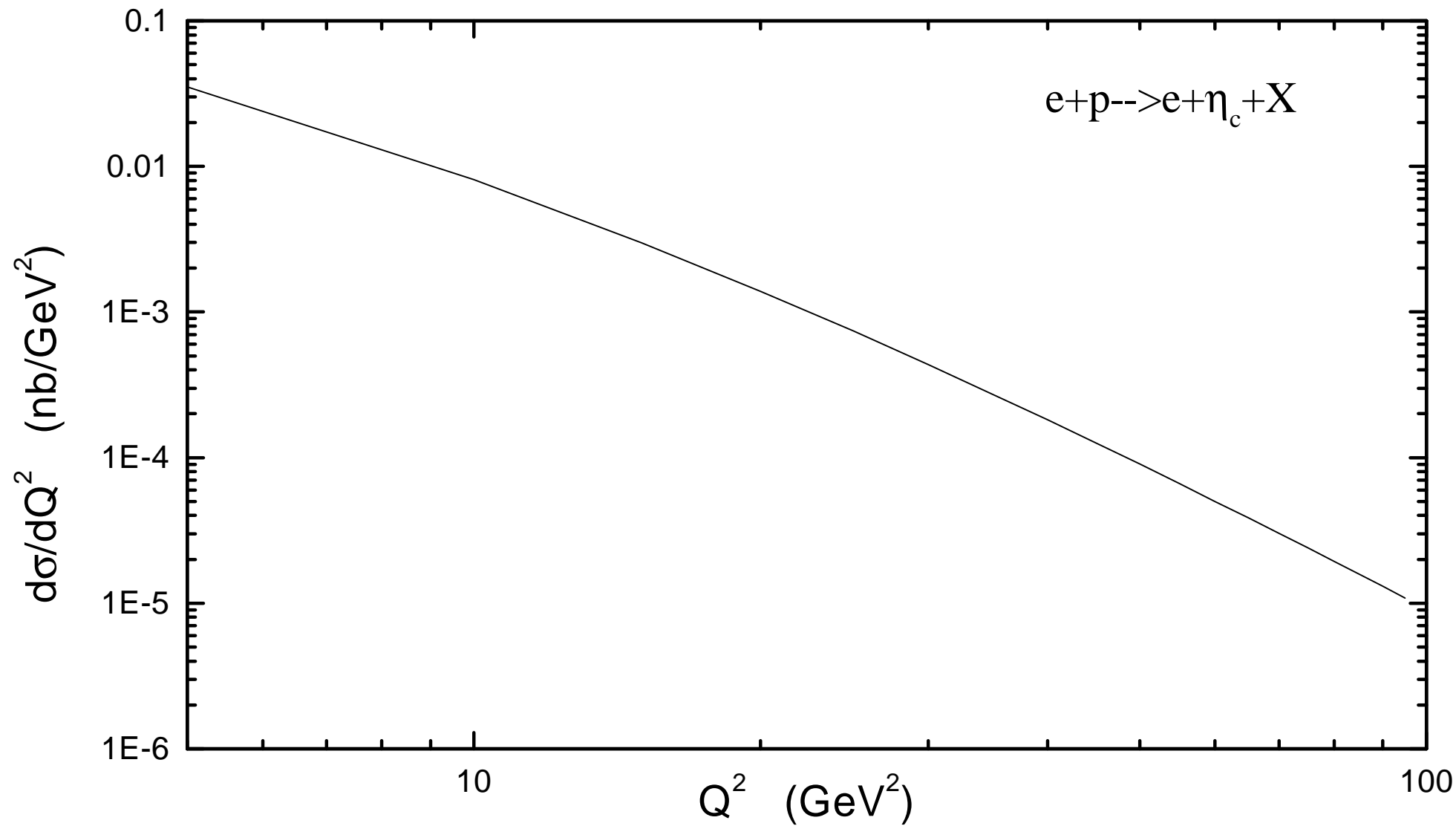


Fig.2

$$\gamma^* + p \rightarrow \eta_c + X \quad (W_{\gamma p}^* = 100 \text{ GeV})$$

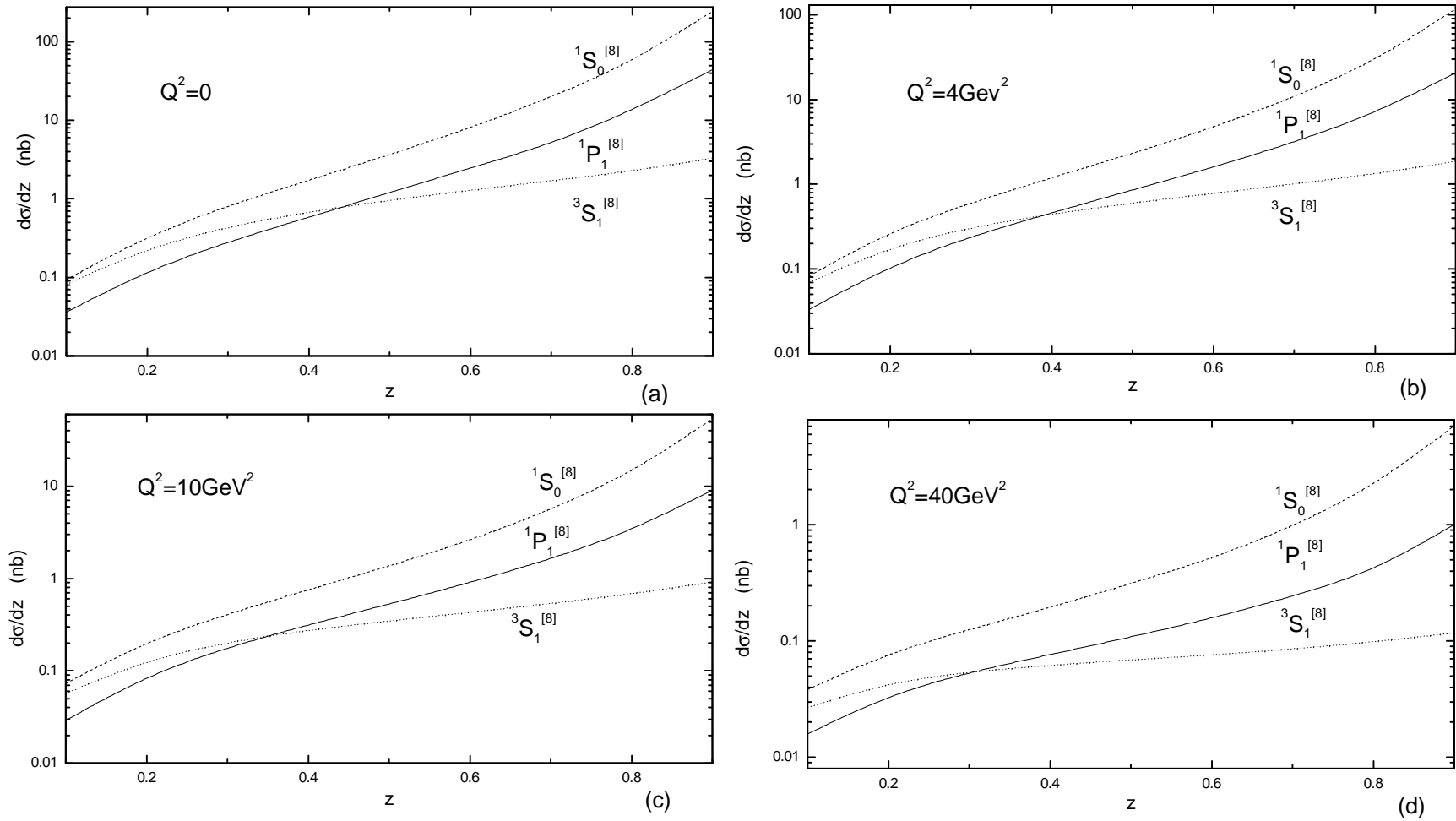


Fig.3

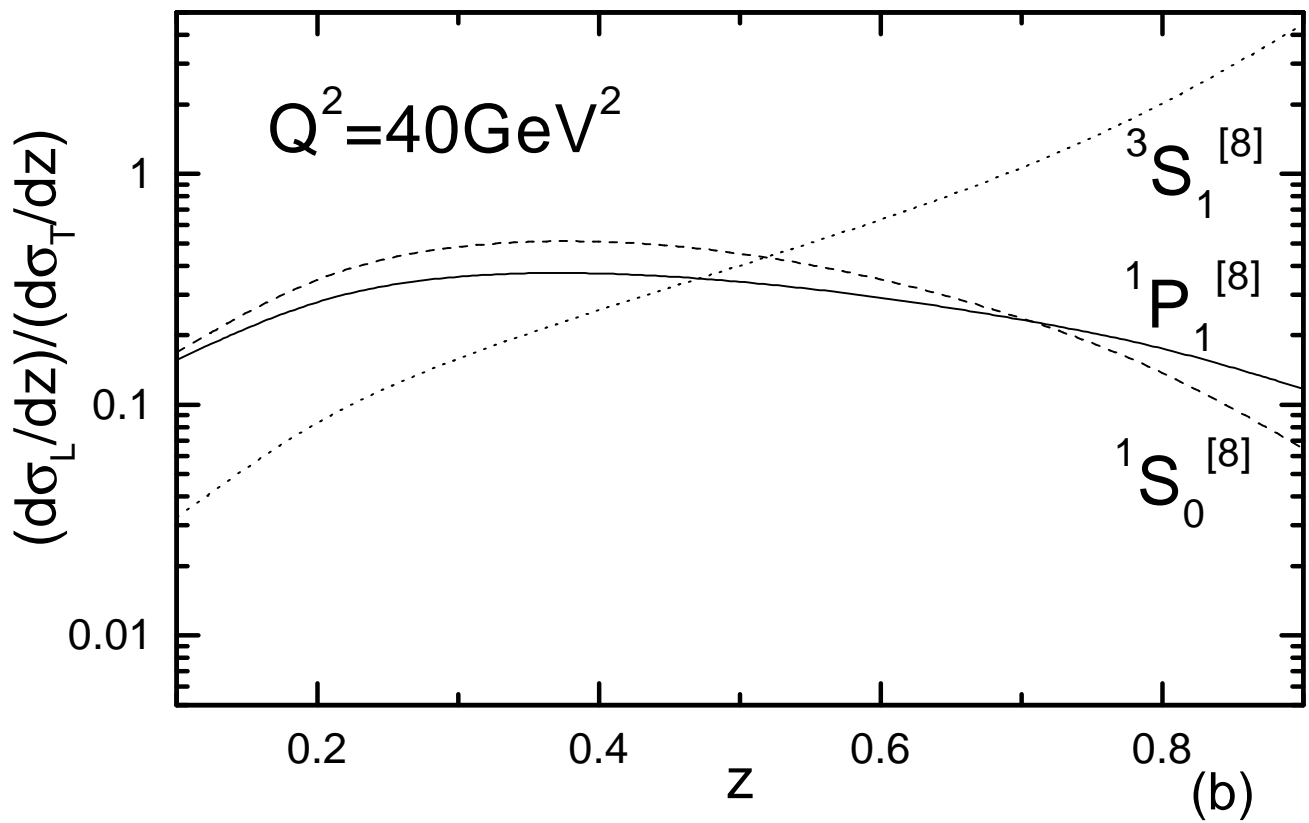
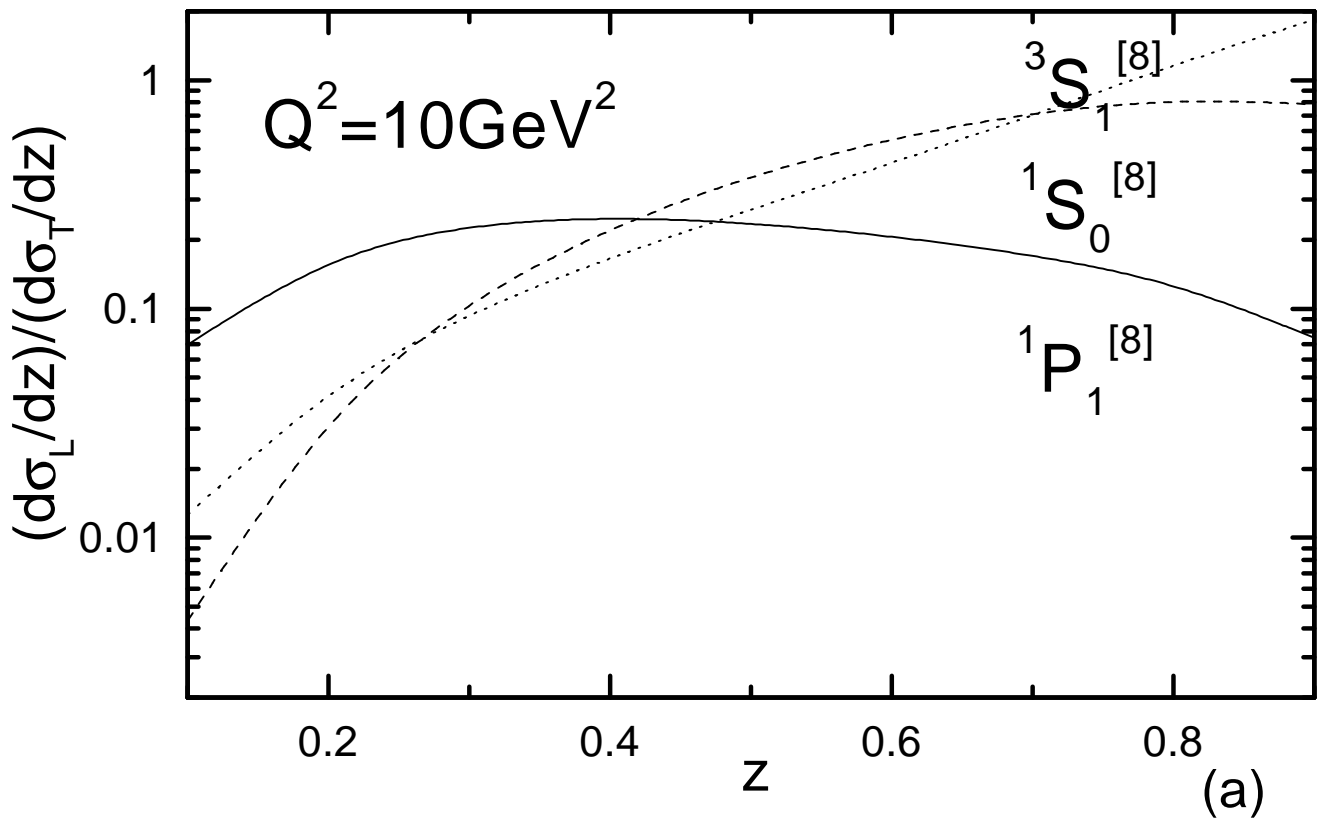


Fig.4

$e+p \rightarrow e+\eta_c+X$ ($E_{\text{m.c.}}=300\text{GeV}$)

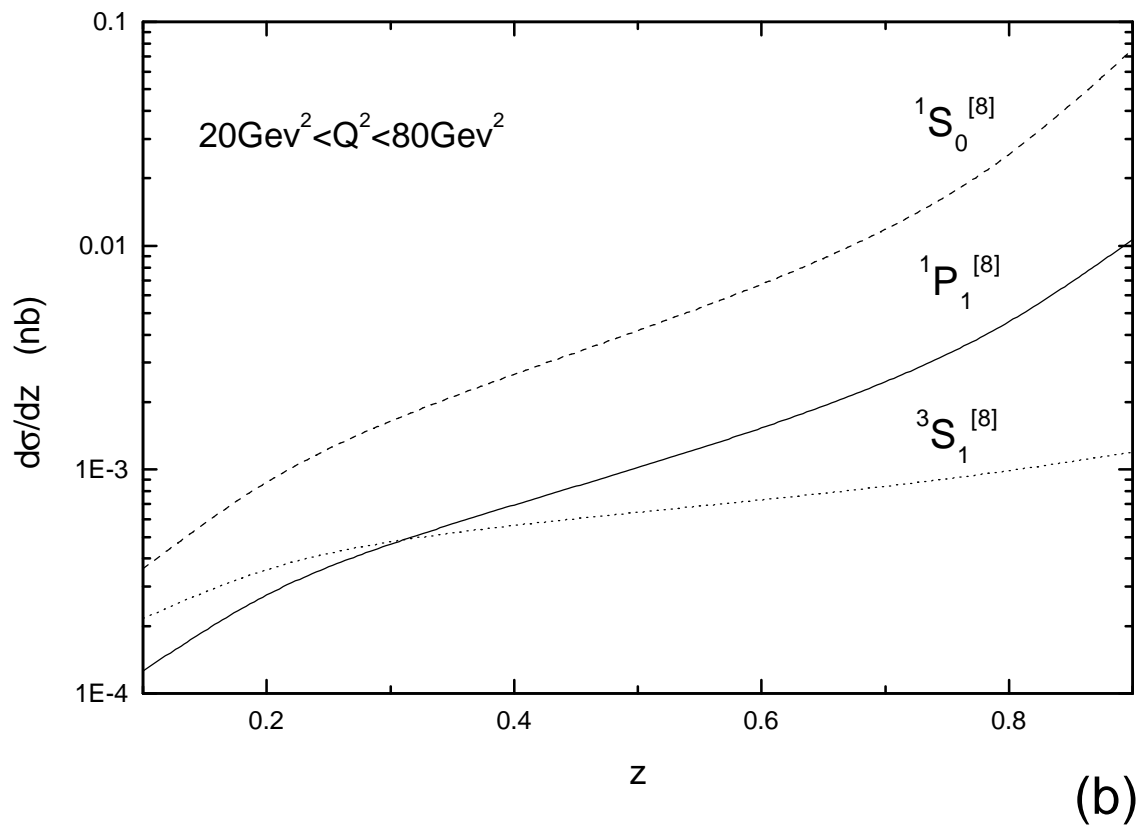
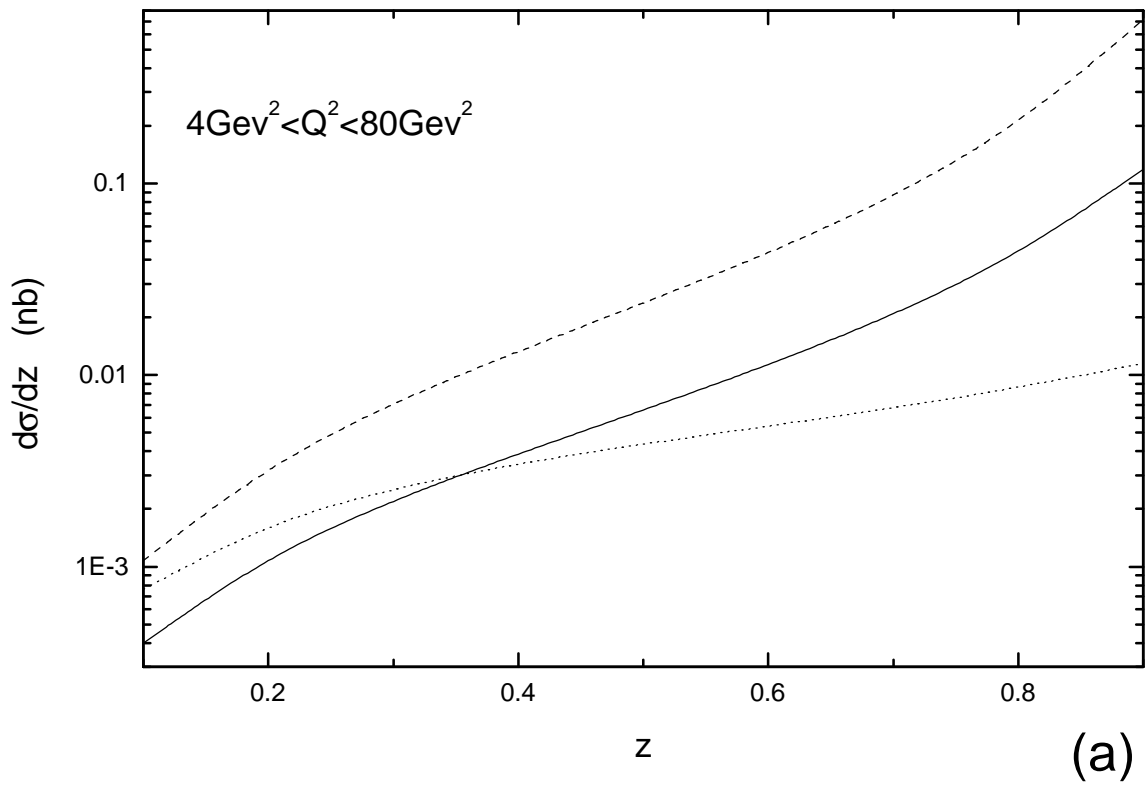


Fig.5